



**HAL**  
open science

# A combined DGT - DET approach for an in situ investigation of uranium resupply from large soil profiles in a wetland impacted by former mining activities

A. Martin, Gilles F Montavon, Catherine Landesman

## ► To cite this version:

A. Martin, Gilles F Montavon, Catherine Landesman. A combined DGT - DET approach for an in situ investigation of uranium resupply from large soil profiles in a wetland impacted by former mining activities. *Chemosphere*, 2021, 279, pp.130526. 10.1016/j.chemosphere.2021.130526 . hal-03233404

**HAL Id: hal-03233404**

**<https://hal.science/hal-03233404>**

Submitted on 24 May 2021

**HAL** is a multi-disciplinary open access archive for the deposit and dissemination of scientific research documents, whether they are published or not. The documents may come from teaching and research institutions in France or abroad, or from public or private research centers.

L'archive ouverte pluridisciplinaire **HAL**, est destinée au dépôt et à la diffusion de documents scientifiques de niveau recherche, publiés ou non, émanant des établissements d'enseignement et de recherche français ou étrangers, des laboratoires publics ou privés.

1 **A combined DGT - DET approach for an *in situ* investigation of Uranium resupply**  
2 **from large soil profiles in a wetland impacted by former mining activities**

3 A. Martin<sup>a</sup>, G. Montavon<sup>a,b</sup>, C. Landesman<sup>a\*</sup>

4 <sup>a</sup> SUBATECH, UMR 6457 (IMT-Atlantique, Université de Nantes, CNRS-IN2P3),  
5 4 Rue Alfred Kastler, 44307 Nantes, France

6 <sup>b</sup> LTSER “Zone Atelier Territoires Uranifères”, 63000 Clermont-Ferrand, France

7  
8 \*Corresponding author: Phone: + 33 2 51 85 84 13; Email address:

9 catherine.landesman@subatech.in2p3.fr

---

10  
11 **Highlights**

- 12 - A combination of 5 DET and DGT was deployed in the Rophin wetland soil layers.  
13 - The metal resupply was assessed by calculating the R ratio ( $R = [U]_{DGT}/[U]_{\text{pore water}}$ ).  
14 - A R value of 0.87 demonstrates the resupply of U from a mine deposit layer.  
15 - Up to 1,750 mg kg<sup>-1</sup> U are retained in wetland topsoil by organic complexation.  
16 - A change in red-ox sensitive elements occurs below the soil-water interface.

17  
18 **Abstract (250 words)**

19 An *in situ* methodology combining DET and DGT probes was applied in a wetland soil,  
20 downstream of a former uranium mine (Rophin), to evaluate metal resupply by calculating  
21 the R ratio ( $R = [U]_{DGT}/[U]_{\text{pore water}}$ ) from a high resolution and large (75 cm) soil profile. Our  
22 study confirms its applicability in soil layers with varying properties; only soil layers with  
23 low water content or coarse texture appear to be limiting factors. For soil profiles, DET  
24 provides new insights of the distribution of Uranium as soluble species (free ions, small  
25 inorganic complexes,...) along the pore water profile, whereas DGT highlights the presence  
26 of other “DGT labile” species. The pairing of DET and DGT, plus the calculation of the R,  
27 highlights two U behaviors in combining results from red-ox sensitive elements (Mn, Fe).  
28 First, in the organic topsoil layer, an increase in  $[U]_{DET}$  and  $[U]_{DGT}$  at 3-4 cm reflects the  
29 desorption of U probably trapped onto Fe- and Mn-oxohydroxides in a DGT-labile form.

30 However, the resupply from soil to pore water is close to a diffusion only case ( $R < 0.2$ )  
31 meaning that a portion of U is certainly tightly bound by OM in soil as non-labile species.  
32 Second, a peak in  $[U]_{DGT}$  perfectly corresponding to the former mine deposit layer signifies  
33 the presence of U under DGT-labile species. Moreover, a maximum R values of 0.87  
34 demonstrates the near complete resupply of U from a labile fraction in this layer, as opposed  
35 to other elements like Pb.

36

37 **Keywords (6 words):** Uranium, DGT, DET, lability, soil, mine

38

39

#### 40 1. Introduction

41 Understanding the fate of radionuclides in the vicinity of former uranium (U) mines is of  
42 great importance given both the potential enhancement of environmental dose rates and the  
43 transfer of radionuclides into ecosystems. Uranium concentrations may locally exceed  
44 natural background levels in the vicinity of former U mining sites (Fuller et al. 2020,  
45 Chautard et al. 2020, Lottermoser and Ashley 2005, Martin et al. 2020), particularly in  
46 natural and artificial wetlands such as peats and flooded soils (Stetten et al. 2018, Wang et  
47 al. 2014, Wang et al. 2013, Schöner et al 2009). All information on the geochemical  
48 speciation and dynamics of U in soils for the purpose of regulating U transfer into other  
49 environmental compartment is therefore of major interest.

50 The mobility of U in soils and sediments is mainly driven by redox processes, ligand  
51 complexation, sorption (on Fe-Mn-oxohydroxides and clay) and (co)-precipitation processes  
52 (Stetten et al. 2018, Schöner et al. 2009, Sajih et al. 2014). A simple approach to  
53 summarizing the geochemical speciation of metal in soils consists of considering its presence  
54 in the soil solution (pore water) as free ions, complexes with inorganic or organic ligands,  
55 associated with colloids (inorganic or organic as well), and tightly bound and/or  
56 exchangeable species in the soil solid phase (Guan 2019, Davison 2016). Stetten et al. (2018)  
57 recently investigated the speciation of U in a wetland impacted by a seasonally flooded mine  
58 using both the XANES and EXAFS techniques. They demonstrated that U speciation is  
59 driven by the water table level, which marks the limit between oxic and anoxic environments

60 as well as the associated presence of  $U_{VI}$  and  $U_{IV}$  species.  $U_{IV}$  is generally expected to be a  
61 low-mobility U species, existing as precipitated  $UO_2$ , in contrast with  $U_{VI}$  species, which are  
62 typically soluble and mobile (Wang et al. 2013, Fuller et al. 2020). However, recent studies  
63 (Wang et al. 2013, Stetten et al. 2018) conducted in the pore water of mine-impacted peat  
64 demonstrated the presence of mobile  $U_{IV}$ -bearing colloids (500 kDa - 0.22  $\mu$ m) composed  
65 of  $Fe(OH)_2$  and organic matter (OM).

66 In addition to studying the geochemical properties of U, it is important to evaluate transfers  
67 to the biotope. It is well-known that the plant uptake of potentially toxic elements in soils is  
68 correlated with the exchangeable metal pool rather than with the total metal soil  
69 concentration. Therefore, increasing interest has been shown in quantifying the labile  
70 fraction by a variety of techniques that speciate U in soils and sediments (Duquene et al.  
71 2010, Kohler et al. 2004, Leermakers et al. 2016, Gao et al. 2010, Bond et al. 2007, Zachara  
72 et al. 2007, Ahmed 2014). Such techniques however were mainly developed for laboratory  
73 experiments from dry soil samples, thus resulting in the *in situ* environmental conditions that  
74 drive U mobility being partially reproduced. Among these techniques, Diffusive Gradient in  
75 Thin film (DGT) is the only dynamic technique to be successfully applied *in situ* on soils  
76 and sediments.

77 DGT and DET (Diffusive Equilibrium in Thin film) (Zhang and Davison 1995, Krom 1994)  
78 have been widely used to sample trace metals in various environments (fresh and salty  
79 waters, pore water of sediments or soils) due to some key advantages: rapid equilibration  
80 time vs traditional sediment peepers (mean equilibration time < 1day for DET and 1 to 3  
81 days for DGT, Peijnenberg et al 2014), robustness, ease of deployment, and minimal  
82 disturbance in the field. DGT and DET mainly measure free ions, small inorganic complexes  
83 and a number of organic complexes, whose dissociation rate is fast compared to the diffusion  
84 time scale in both diffusive and resin gels. However, within a typical deployment time (hours  
85 to days), DGT is unable to measure most colloids since they diffuse much more slowly than  
86 free ions in the diffusion layer (Guan 2019, Davison 2016).

87 The DGT-induced local depletion of metal concentration in pore water causes the release of  
88 species from the readily exchangeable fraction in the soil solid phase. The pool initially  
89 present in pore water plus the DGT-induced pool both contribute to the quantity measured  
90 by DGT. The magnitude of the flux measured by DGT is determined by: the concentration  
91 in pore water, the rate of diffusion, and the rate of resupply from both the solid phase and

92 complexes in pore water. These “DGT labile” species are correlated with the time available  
93 for complexes to dissociate in pore water and fractions to desorb from the solid phase.  
94 Consequently, a DGT measurement integrates all soil properties into a single key parameter,  
95 namely the DGT-labile concentration ( $C_{DGT}$ ) or flux (Guan 2019). The R ratio ( $R=C_{DGT}/C_{pore}$   
96  $_{water}$ ) is thus a good indicator of the soil’s capability to resupply metal (labile fraction) to  
97 DGT.

98 While applications of a DET/DGT combination to U and other metals in sediments were  
99 initiated 14 years ago (Gao et al. 2006, Monbet et al. 2008, McKelvie and Worsfold 2008,  
100 Pradit et al. 2013, Leermakers et al. 2005), studies on soils are scarce and have mostly been  
101 performed under laboratory conditions (Hooda et al. 1999, Nowack et al. 2004, Koehler and  
102 Schulin 2004) due to both the water saturation conditions required to ensure smooth  
103 operations and the complexity of field experiments. Moreover, DGT probes were mainly  
104 used in their original 15-cm design length, which is adapted to studying the water-sediment  
105 column interface but less convenient for studying a complex soil profile. To the best of our  
106 knowledge, Leermakers *et al.* (2016) reported the first *in situ* deployment of DGT samplers  
107 in a U-contaminated soil, with use of a DGT holder yielding a high resolution profile over a  
108 75-cm depth.

109 In this study, a combination of DET and DGT probes was simultaneously deployed *in situ*  
110 within a particularly interesting wetland featuring an anthropogenic anomaly (Martin et al.  
111 2020, Roux et al. 2020). The main objective of this work is to determine the lability of U  
112 according to soil characteristics as well as the origin of the contamination. Moreover, this  
113 paper presents new data for U in pore water with a large 75-cm vertical depth relative to the  
114 characteristics of the corresponding soil profiles. Results emphasize the complementary  
115 nature of DGT and DET, in comparison to other methods for assessing U pore water  
116 composition. Soil concentrations of mine activity-related elements (U and Pb), along with  
117 fluxes of elements from the soil-water interface to DGT, was assessed by calculating the R  
118 ratio, as derived from the combined DGT and DET measurements. These results were  
119 corroborated by the measurement of red-ox sensitive elements (Mn and Fe) in order to better  
120 understand the geochemical processes involved.

## 121 2. Materials and Methods

## 122 2.1. Study site

123 The history, geology and hydrogeology of the Rophin tailings storage site have been  
124 described elsewhere (Martin et al. 2020, Roux et al. 2020). As a brief background, the U ore  
125 of Rophin, mainly parsonsite ( $\text{Pb}_2(\text{UO}_2)(\text{PO}_4)_2 \cdot 2\text{H}_2\text{O}, \text{U}_{\text{VI}}$ ), was mined from 1949 to 1955  
126 using an ore washing plant process and associated settling ponds that continued to operate  
127 until 1957 with pitchblende ( $\text{UO}_2, \text{U}_{\text{IV}}$ ) from the ‘Bois-Noirs’ mine. Nowadays, the storage  
128 site is covered by a vegetated soil, and forest vegetation is growing at the top of the mine  
129 waste storage heap. Soil cores extracted in the nearby wetland (200 m downstream) show  
130 high U concentrations, which appear to be associated with the presence of a whitish silt loam  
131 soil layer located at a depth of around 10-30 cm, below an organic topsoil layer. These high  
132 U concentrations have been ascribed to a discharge of U mineral particles, transported by  
133 turbid water, due to a malfunction in both the ore washing plant process and the  
134 sedimentation step. In addition to the U contamination identified in this anthropogenic layer,  
135 U is also found to be trapped in the high OM content topsoil layer. Our interest is therefore  
136 to estimate the potential lability of U in these layers. A general map of the Rophin watershed  
137 (Puy de Dôme, France) and its mapping by gamma-ray dose rate, is presented in Fig. 1.

## 138 2.2. Principles of DGT and DET use in soil

139 The principles of DET and DGT techniques are widely discussed in the literature (Davison  
140 2016). While the DET probe accesses free metal, metal complex and free ligand species in  
141 soil pore water through equilibration of solutes within a diffusion layer (consisting of  
142 hydrogel plus filter membrane), the DGT probe measures the flux of solutes (through the  
143 same diffusion layer) from the soil pore water to a binding layer (Chelex<sup>®</sup> resin embedded  
144 in hydrogel).

145 Flux depends on: i) the concentration gradient (due to the binding layer) existing on both  
146 sides of the diffusion layer, and ii) the ability of the soil to resupply solutes when their  
147 concentrations become depleted. The solute flux can be interpreted as the time-averaged  
148 concentration at the probe surface during deployment and is calculated according to  
149 Equation 1 (derived from Fick's first law):

$$C_{\text{DGT}} = m_U \Delta_{\text{gel}} / (D_{\text{gel}} \text{At}) \quad (1)$$

150 where  $m_U$  is the mass of U eluted from the Chelex<sup>®</sup> resin ( $\mu\text{g}$ ), corrected for the elution factor  
151 ( $f_e$ ),  $\Delta_{gel}$  the total thickness of the diffusive gel layer and protective membrane filter ( $\Delta_{gel} =$   
152  $0.905 \pm 0.0014$  mm),  $D_{gel}$  the temperature-corrected diffusion coefficient of U through the  
153 diffusive gel layer ( $\text{cm}^2 \text{ s}^{-1}$ ) using the Stokes-Einstein Equation,  $A$  the exposure area  
154 (sampling window), and  $t$  the deployment time. For  $D_{gel}(\text{U})$ , a mean value derived from  
155 Gregusova and Docekal (2011) associated with a larger uncertainty accounting for  
156 discrepancies in the literature values has been chosen ( $D_{gel} = 4.39 \pm 0.40 \times 10^{-6} \text{ cm}^2 \text{ s}^{-1}$  at  
157  $25^\circ\text{C}$  and  $\text{pH} = 6.4$ ). This value is in good agreement with those reported in several studies  
158 Turner et al. 2012, Drozdak et al. 2015, 2016). The quantitative determination by ICP-MS  
159 requires a reproducible elution of metals trapped in the Chelex<sup>®</sup> resin. The elution factor of  
160 U was experimentally determined to equal  $0.84 \pm 0.04$  under our experimental conditions  
161 (data not shown). For the other metals (Mn, Fe and Pb), the values of elution factors and  $D_{gel}$   
162 were drawn from Davison (Davison 2016) (Table S2).

163 The R ratio values ( $R = C_{\text{DGT}}/C_{\text{pore water}}$ ) highlight three cases that arise with respect to the  
164 DGT-measured flux and interfacial concentration in soil. When the U flux from soil to pore  
165 water (resupply) effectively buffers the pore water concentration ( $R > 0.8$ ; sustained case),  
166 DGT concentration is close to the true U pore water concentration as regards DGT labile  
167 species. However, when the U resupply is limited ( $0.2 \leq R \leq 0.8$ ; partially sustained case) or  
168 nonexistent ( $R < 0.2$ ; diffusion only case), the U concentration measured by DGT is less  
169 than the actual U pore water concentration, with both DGT-labile and inert species being  
170 present in the soil (Davison 2016 and references herein).

### 171 2.3. Preparation of DGT and DET probes in the laboratory

172 DGT and DET probes were purchased from DGT Research<sup>®</sup>. They consisted of plastic  
173 holders with overall dimensions of  $24 \times 4 \times 0.5$  cm with a  $1.8 \times 15$ -cm open window. DGT  
174 probes (LSPM model) were composed of a Chelex<sup>®</sup>-100 binding layer (0.4 mm) with an  
175 area of  $27 \text{ cm}^2$ , a polyacrylamide diffusive gel ( $\Delta g = 0.78$  mm) and a polyethersulfone filter  
176 (PES) membrane ( $0.45 \mu\text{m}$ ). DET-constrained probes were of the LCP model with 75 slits  
177 ( $1 \times 1 \times 1.8$  mm) on the base plate filled with agarose diffusive gel and covered by a  $0.45$ -  
178  $\mu\text{m}$  PES filter membrane (Zhang and Davison 1995).

179 In order to minimize any redox disturbance during deployment in soil, the DGT and DET  
180 probes were first conditioned in a glove box under argon atmosphere. The probes were

181 immersed in a deoxygenated 0.01 M NaNO<sub>3</sub> solution containing 2.5 g.L<sup>-1</sup> Chelex<sup>®</sup> resin to  
182 remove any trace metals (Davison 2016) and allowed to rest for at least 24 h with bubbling  
183 argon gas. The DGT and DET samplers were stored at 4°C in a tight plastic bag containing  
184 a few drops of 0.01 M NaNO<sub>3</sub>; they were then transported to the site in a container filled  
185 with argon gas.

186 After deployment, the probes were disassembled in the laboratory, and the DGT Chelex<sup>®</sup>  
187 binding phase was sliced at 1-cm intervals with a ceramic blade. The slices were inserted  
188 into pre-weighed vials and reweighed in order to obtain sample weight and, hence, the  
189 volume and surface area. DET agarose gels were also placed into pre-weighed vials and  
190 reweighed to derive gel volume. A compromise on both spatial resolution and method  
191 detection limit was struck by placing five DET slices in the same elution vial to ensure the  
192 same spatial scale as DGT (1 cm). The DGT and DET gel slices were separately soaked in  
193 1 mL of 1 M HNO<sub>3</sub> for at least 24 h before analysis of the eluate by ICP-MS.

#### 194 *2.4. Field deployment*

195 Field deployment took place in the wetland zone downstream of the former Rophin U mine  
196 (3°33'0.27"E and 46°0'25.23"N) in April 2018 and lasted 24 h (a complementary study was  
197 performed in November 2018). The chosen sampling area is a fully saturated zone (Fig. S1  
198 a and b) characterized by the highest measured gamma dose rates.

199 A specific PVC holder was constructed to obtain continuous profiles up to 75 cm deep (equal  
200 to 5 probe lengths). This holder differs from Leermaker's study (Leermakers et al. 2016) by  
201 integrating DGT/DET probes in a back-to-back position (Fig. S3). On-site, the probes were  
202 removed from their container and quickly placed in the PVC holder, which was first  
203 manually driven into the soil to a 20-cm depth and then with a mallet up to 75 cm.

204 At the end of their deployment (24h), the probes were retrieved, wiped to remove any  
205 adhering soil particles, rinsed with ultrapure water and finally stored in sealed plastic bags,  
206 along with a few drops of 0.01 M NaNO<sub>3</sub> to maintain water saturation and prevent the gels  
207 from drying.

208 A triplicate of DGT (in the piston configuration) was used as a blank in following all steps  
209 of the protocol (including the cutting step) except for deployment. After disassembly, their  
210 diffusive and binding gels were considered as a blank for the DET and DGT probes,



211 respectively. Lastly, soil temperature gradients were measured every 10 cm over a 120-cm  
212 depth with a 1.5-m long temperature probe equipped with an LCD display (Agreto®).

### 213 2.5. Soil sampling and characterization

214 After retrieval of the DET/DGT probes, soil samples were collected at the exact same  
215 location. The sampling area was covered by approx. 2 cm of water, in assuming fully  
216 saturated soil layers in the wetland at the beginning of spring 2018 (Fig. S1). Semi-  
217 cylindrical soil cores (50 × 10 cm) were sampled with a Russian-type corer (Eijkelkamp®  
218 Soil & Water) and subdivided into soil samples according to apparent soil layers. Wet soil  
219 samples were then divided into two parts, one dried at 105°C and then sieved at 2 mm the  
220 other frozen at -18°C. In addition, pore water samples were collected using both in-field-  
221 based methods (DET, suction lysimeter) and laboratory methods (centrifugation, soil  
222 suspensions) for purposes of comparison. Details on the methods and results are available in  
223 Table S4.

224 Soil pH was measured according to the NF ISO 10390 method. Five grams of dry soil  
225 samples were vigorously shaken with 25 ml of UP water for 5 min (1:5 soil/water). The  
226 suspension was then left to rest at least 4 h before pH measurement (CyberScan pH 110  
227 meter, Eutech Instruments) using an electrode dedicated to viscous media. The supernatants  
228 were then filtered at 0.45 µm, acidified and stored at 4°C until ICP-MS analysis. Water and  
229 organic matter contents were determined by loss of ignition. The procedure followed was  
230 that specified in Heiri et al. 2001, Lotter and Lemcke 2001. Between 5 and 10 g of  
231 homogenized wet samples were introduced into porcelain crucibles and first dried at 105°C  
232 overnight in a furnace (Nabertherm, Inc.), before being heated to 550°C for 4 h in order to  
233 burn the organic matter. After each temperature step, the crucibles were cooled to room  
234 temperature in a desiccator and weighed. The particle size distribution of non-organic soil  
235 samples was determined by laser granulometry (Mastersizer 3000 with a Hydro LV  
236 dispersion system, Malvern Panalytical®). Soil texture was determined according to particle  
237 size distribution and USDA definition (Fig. S5).

238 Prior to ICP-MS analysis, dry soil samples sieved to 200 µm were mineralized by  
239 microwave-assisted digestion using a Multiwave 3000 microwave (Anton Paar). A 7.5:1.5:1  
240 mixture of HCl (36% vol.), HNO<sub>3</sub> (68% vol.) and HF (47% vol) concentrated acids was  
241 added to around 100 mg of sieved soil in a cleaned PTFE reactor. The mixture was then

242 heated at 600 W for 40 min. After cooling, 5 mL of a saturated solution of  $\text{H}_3\text{BO}_3$  in  $\text{HNO}_3$   
243 (7.5 M) was added to neutralize the HF, and the mixture was heated a second time. The total  
244 soil sample mineralization was visually checked, and the liquid phase was transferred into  
245 tubes. Ultrapure water (10 mL two times) was added for further dilution and analysis.  
246 Additional X-ray diffraction (XRD) analyses were performed on dry soil powder using a  
247 Pananalytical Empirean diffractometer running with a  $\text{Cu-K}\alpha_1$  radiation ( $\lambda=1.5406\text{\AA}$ ). XRD  
248 patterns were recorded in the  $5\text{-}80^\circ 2\Theta$  interval with a  $0.013^\circ 2\Theta$  step size.

## 249 2.6. Analysis

250 Anion ( $\text{F}^-$ ,  $\text{Cl}^-$ ,  $\text{SO}_4^{2-}$ ,  $\text{NO}_3^-$ ,  $\text{Br}^-$ ,  $\text{PO}_4^{3-}$ ) and cation ( $\text{Na}^+$ ,  $\text{K}^+$ ,  $\text{Mg}^{2+}$ ,  $\text{Ca}^{2+}$ ) analyses were  
251 performed on pore water samples by ion chromatography (850 Professional IC, Dionex and  
252 ICS-1000 IC, Metrohm). Physicochemical parameters such as temperature, pH and Eh were  
253 measured *in situ* using a CyberScan pH 110 meter (Eutech Instruments) coupled with  
254 dedicated probes.

255 Element concentrations (U, Mn, Fe and Pb) were analyzed by Single Quadrupole Inductively  
256 Coupled Plasma-Mass Spectrometry (ICP XSERIES 2, ThermoFisher Scientific). A  
257 collision chamber mode (addition of H/He gas) was used for the Fe analysis. Matrix effects  
258 were minimized by diluting the samples in 2% bi-distilled  $\text{HNO}_3$  (v/v). DET and DGT  
259 eluates were diluted by factors of 20 and 50, respectively, or until 1,000 (for DGT eluates  
260 with high concentrations). The analytical LQ for the DGT, DET and pore water samples of  
261 each element are given in Table S2 according to field blanks for DGT and DET. Analytical  
262 uncertainties are expressed as a confidence interval ( $\alpha = 0.05$ ). In pore water samples, the  
263 [U] mean uncertainty is around 15%. For each metal (U, Mn, Fe and Pb), DET and DGT  
264 concentrations and R calculation's uncertainties were calculated according to Gauss'law of  
265 error propagation ( $k=2$ ). More precisely, for Uranium, the following mean values were thus  
266 obtained: 17% (DET), 25% (DGT) and consequently, 32% for R-values

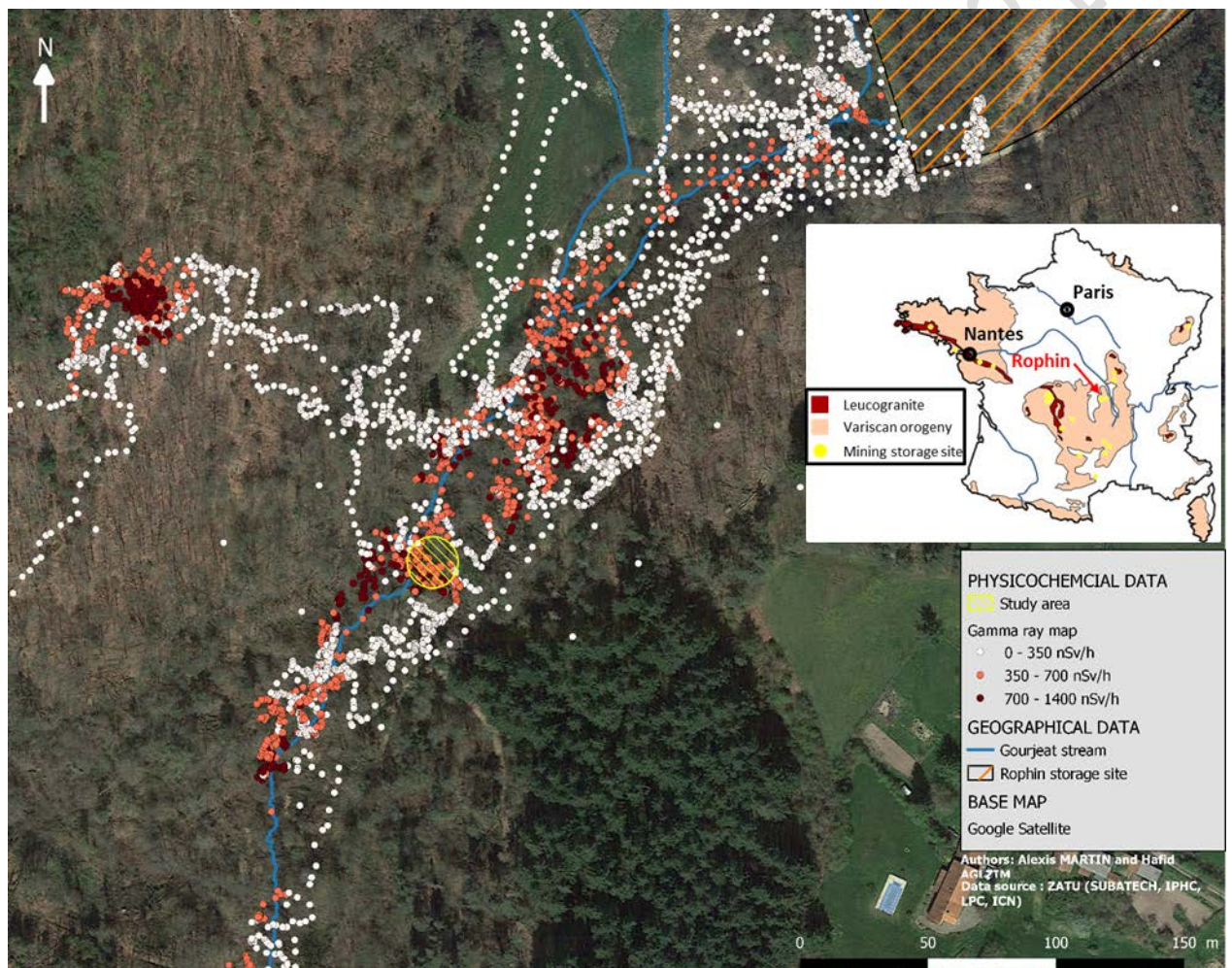
267 For all techniques used, quantification of trace metal concentrations (ICP-MS) and major  
268 ions (IC) were based upon calibration curves prepared from multi-element or single element  
269 standard solutions (SCP Science, Canada). Inter-laboratory standard materials (BIPEA)  
270 were used to verify the accuracy of all analytical protocols.”

271

## 272 3. Results and Discussion

273 3.1. Soil properties and chemical characteristics

274 Variation in the water table level (related to a high/low flow cycle) in the DGT sampling  
275 area was measured at +2 to -23 cm (with 0 cm at the soil surface) in April 2018 and  
276 November 2018, respectively. In April 2018, the wetland was fully saturated (Fig. 1);  
277 consequently, each soil layer was considered at its maximum water holding capacity.  
278 Moreover, the O<sub>2</sub> profile measured over the first 3 cm decreased sharply from 100% O<sub>2</sub>  
279 (overlying water) to 2% at 1.5 cm (Fig. S6), with no oxygen being present below this depth.



280

281 Figure 1: Location of the Rophin site in the context of mining storage in France (adapted from  
282 AREVA NC., 2009), gamma-ray dose rate mapping of the site in 2018 (colored dots) and wetland  
283 location (yellow circle).

284

285 The soil layer properties are listed in Table 1. pH values are characteristic of a wooded  
286 wetland and range from 4.06 to 4.90 (average 4.5). Six layers (L1 to L6) can be

287 distinguished, based on visual observations. Some are typical of wetlands, rich in organic  
288 matter (i.e. L1), while others are associated with the history of site mining operations (i.e.  
289 L3, L4). These layers were sorted into 4 main types (Baize and Girard 2008): “histosol layer”  
290 (H-type layer), “humus layer” (O-type), “organo-mineral layers” (A-type), and “technosol  
291 layer” (Z-type). Mixed layers (L2-4 and L3-4) were also observed but not sampled due to  
292 their heterogeneity and the likely complexity of any subsequent interpretation.

293 A rapid qualitative description of the soil profile is given below:

- 294 - The H-type layer (L1) is mainly composed of fibrous soil material and roots, which  
295 confers a black color, very low bulk density (0.17) and high water holding capacity  
296 (85%). The organic matter carbon content is the highest of the entire soil profile at  
297 47.5% of the dry soil.
- 298 - The A-type layer consists of two different layers, Ag and A, both combining organic  
299 and mineral characteristics (L2, L5). The Ag and A layers share common  
300 characteristics, i.e. an intermediate water content (36% and 45%), a low level of  
301 organic matter (3.0% and 3.2%) and a silt loam texture. The orange color of the Ag  
302 layer suggests the occurrence of an oxidative process (precipitation of Fe-  
303 oxohydroxides).
- 304 - Z-type layers (L3, L4) are distinguished as fine (f) and sandy (s) depending on their  
305 texture, bulk density and particle size distribution (Table 1 and Fig. S5). These layers  
306 are characterized by high U concentrations (1,840 and 790 mg.kg<sup>-1</sup>) and low organic  
307 contents (2.6% and 1.2%, respectively). Such high U concentrations, along with the  
308 abundance of finer larger particles, suggest that these layers are constituted of  
309 crushed extracted materials that had settled into the former Rophin mine ponds.  
310 According to Martin et al. (2020), these mining residues were released into the  
311 Rophin watershed, thus impacting the wetland under investigation.
- 312 - The O-type layer is the deepest horizon (below 69 cm, L6); it is characterized by a  
313 medium organic carbon content (15.5%) and a brown color highlighting a more  
314 decomposed (degraded) organic matter than that of the H-type layer. This layer  
315 exhibits a low U concentration of around 50 mg.kg<sup>-1</sup>, which is in accordance with the  
316 local geological background. This layer is considered as the soil reference prior to  
317 the period of mining operations and discharge of residues at the Rophin site (Martin  
318 et al. 2020, Roux et al. 2020). Just above the O-layer, the presence of gravels (64 to

319 69 cm) should be noted, thus suggesting the existence of a former creek channeling  
320 mine discharge.

321  
322 Moreover, XRD analysis shows that the soil samples are mainly composed of crystallized  
323 minerals with a small amorphous fraction. In all layers, the mineralogical assemblage is  
324 composed of quartz, alkali feldspars (microcline, orthoclase) and plagioclase (albite-  
325 anorthite) (Fig. S9). These results are consistent with the composition of Rophin stream  
326 sediments reported in Roux et al. (2020).

327

328 Table 1: Description and properties of the main soil layers

Soil layer	Depth (cm)	French type *	pH <sub>soil</sub>	Water content (%)	Organic matter content (%)	Bulk density (kg/m <sup>3</sup> )	Porosity	Soil texture class (USDA)	[U] <sub>soil total</sub> (mg.kg <sup>-1</sup> dry)
L1	0 - 12	H	4.67	85	47.5	0.17	0.87	-	1750 (100)
L2	12 - 18	Ag	4.90	36	3.0	1.08	0.59	Silt loam	430 (30)
L3	25 - 29	Z <sub>f</sub> (fine)	4.45	36	2.6	1.10	0.58	Silt loam	1840 (100)
L4	42 - 49	Z <sub>s</sub> (sandy)	4.56	40	1.2	0.92	0.65	Sandy loam	790 (50)
L5	49 - 64	A	4.06	45	3.2	0.88	0.67	Silt loam	600 (30)
L6	69 - 75	Ob	4.55	54	15.5	0.57	0.58	-	50 (10)

329 \* *Baize and Girard 2008*

330 Such contrasted contamination levels in the soil profile raise questions about the mechanisms  
331 controlling U mobility in this contaminated wetland. However, an investigation of the main  
332 resupply mechanism that leads to the release of U from the L3 soil layer to the pore water  
333 requires additional information on the pore water composition and, more specifically,  
334 dissolved U speciation. Moreover, an investigation of U mobility with the DGT technique  
335 necessitates defining the U concentration in pore water used to calculate the R ratio.

### 336 3.2. *DET and DGT results for uranium depth profiles in soil*

337 In this study, we consider DET to be the most reliable and accurate pore water sampling  
338 method for calculating the R ratio (as suggested in Davison (2016)). DET and DGT actually  
339 feature a very similar design and deployment conditions. Therefore, the filtration of U  
340 species by membrane (< 0.45 μm) and diffusive gel is close for both techniques (free metal,  
341 metal complexes and free ligand species). Moreover, sampling with a field-based method  
342 and high spatial resolution appears to be more relevant in accurately assessing U mobility in  
343 soils. It is well known that concentrations in pore water can be strongly affected by the  
344 methodology employed (Di Bonito et al. 2018, Ullah et al. 2012, Leermakers et al. 2005).

345 This is especially true for redox-sensitive elements such as uranium, as we indeed observed  
346 when comparing the  $[U]_{pw}$  deduced from various sampling methods along the soil profile  
347 with different spatial scales (Table S4). So, the wide range of results observed ( $[U]_{pw}$  from  
348  $50 \mu\text{g.L}^{-1}$  to  $60,100 \mu\text{g.L}^{-1}$  in L3) if used, does lead to bias (by a factor of 1000) R calculation.  
349 Therefore, in the framework of this study, DET results appear to be the most relevant ones  
350 for calculating R ratio. More generally, this issue raises the question about the choice of the  
351 most representative sampling method for characterizing soil's solution since this has a strong  
352 impact on R calculation and its interpretation.

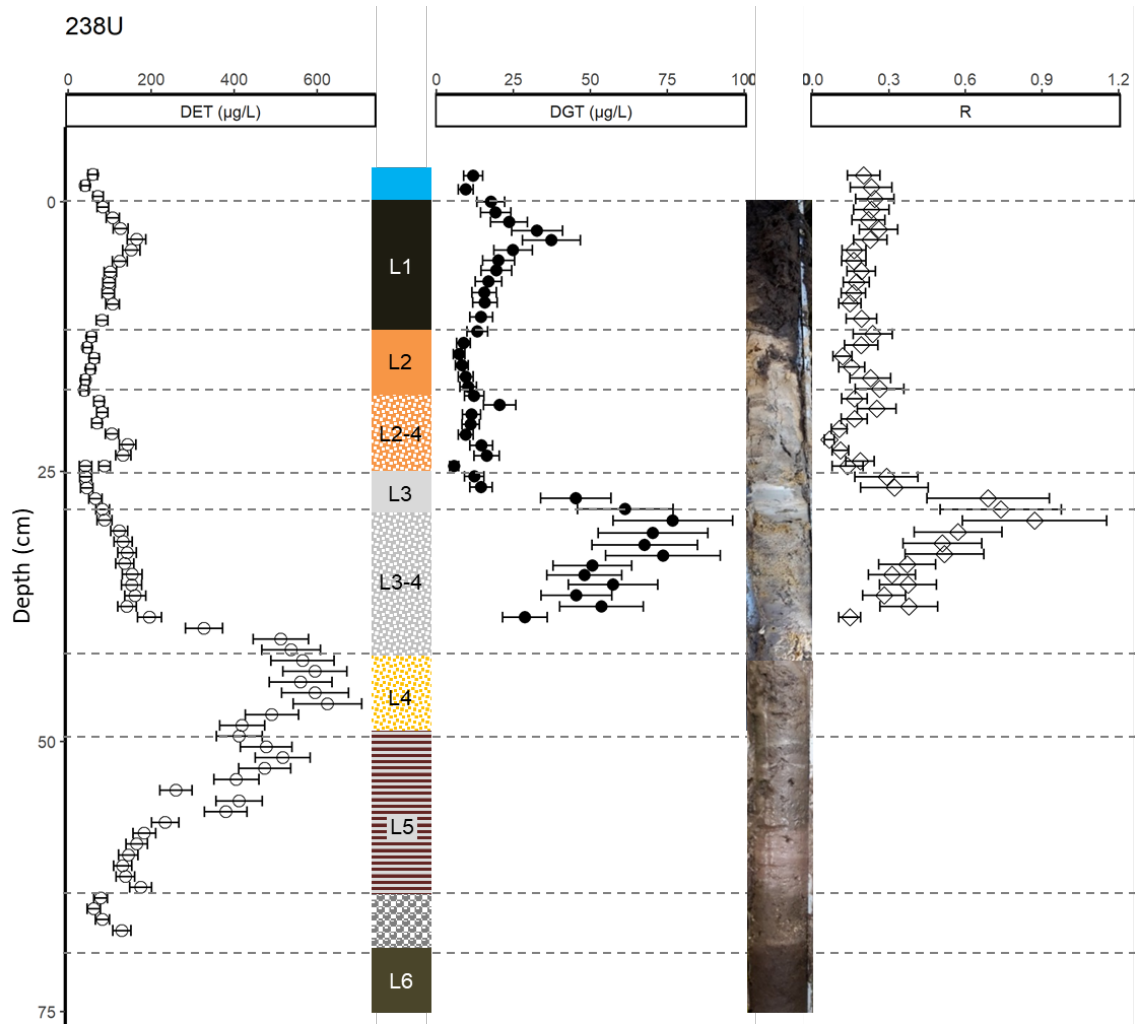
353 The extracts obtained by centrifugation, however, allow adequate water volume for the  
354 physicochemical characterization of pore water (Table S7). In sum, pH values are acidic  
355 (from 3.9 to 6.3), except for the top layer (L1 layer) whose pH value lies close to that of the  
356 overlaying water (pH = 7.2). For ion analysis, high  $\text{SO}_4^{2-}$ ,  $\text{Mg}^{2+}$  and  $\text{Ca}^{2+}$  contents were  
357 observed in pore water from non-organic soil layers and a high concentration of  $\text{F}^-$  was noted  
358 in L4. Under these working conditions, no parameter appears to exert a major influence on  
359 the diffusion coefficients used in DGT calculations (Drozdak et al. 2015, Turner et al.  
360 2012).

361 DET and DGT probes were deployed back-to-back in order to obtain profiles over a 75-cm  
362 depth (Fig. 2). However, DGT results in the 40-75 cm range are missing due to deterioration  
363 of the sampling windows (crumpling and degradation of membranes and/or gel layers). Since  
364 the DGT sampling window is in fact thicker than that of DET (1.32 mm vs. 1.14 mm), its  
365 rubbing against sandy or gravelly soils produced the observed degradation. Fortunately, we  
366 have salvaged the two most interesting soil layers (with the highest U content according to  
367 Martin et al. (2020)), i.e. the surface organic soil layer (L1) and the anthropogenic zone (L3).

368 For DET results over the 75-cm depth, the  $[U]_{DET}$  in pore water range  $[40-625 \mu\text{g.L}^{-1}]$   
369 exhibits a double-peak profile. The main peak ( $625 \mu\text{g.L}^{-1}$ ), located between 36 and 56 cm,  
370 is related to L4 and L5 (top) layers; a second much smaller peak ( $165 \mu\text{g.L}^{-1}$ ) is located at 3-  
371 4 cm (top of the L1 layer). In between these two zones,  $[U]_{DET}$  reaches a minimum ( $40 \mu\text{g.L}^{-1}$ )  
372 in the L2 layer (at a depth of 12-18 cm). Finally, below 64 cm,  $[U]_{DET}$  decreases to low  
373 values ( $< 50 \mu\text{g.L}^{-1}$ ).

374 Regarding the entire depth profile, a wide  $[U]_{DET}$  range is observed. These results highlight  
375 the variation in  $[U]_{pw}$  with respect to the centimeter-scale changes in soil layer properties.  
376 Note that the soil layer nature may have an impact as a coarse texture (sandy loam) may

377 facilitate fluxes from the soil layer to the DET probe and conversely, a fine texture (silt loam)  
 378 may hinder them. Nevertheless, this outcome already reported by Hooda et al. (1999) and  
 379 Docekal et al. (2003) is minimized in the studied saturated soils. Moreover, in any case, DGT  
 380 results will also be affected by this hypothetical bias. Coupling DET and DGT techniques  
 381 will therefore minimize impact on the R ratio calculation.



382

383 Figure 2: Uranium depth profiles obtained from the *in situ* deployment of DET and DGT,  
 384 along with R ratio ( $R = [U]_{DGT}/[U]_{DET}$ ) for a 24h deployment time (errors bars calculated by  
 385 propagating all experimental uncertainties;  $k=2$ )

386

387 For the 40 cm deep DGT profile, the lowest concentration is reached at around 12-26 cm  
 388 with a minimum value of  $7 \mu\text{g.L}^{-1}$ ; moreover, 2 peaks are exhibited. An initial peak, observed  
 389 at around 3-4 cm in the top of layer L1 ( $37 \mu\text{g.L}^{-1}$ ), mirrors the DET profile but with a lower  
 390 peak value. Then, from the end of L3 up to L3-4 (27-40 cm), a second massive peak is  
 391 observed with a maximum at  $77 \mu\text{g.L}^{-1}$ , hence reflecting a higher flux of U to DGT. This

392 second peak could be explained by the existence of readily U DGT-labile species originating  
393 from the high inventory of U in the adjacent L3 layer and conveyed in pore water through  
394 the coarser texture of the mixed L3-4 layer. The ratio between DET and DGT depth profile  
395 results will differentiate the presence of tightly bound and labile U fractions in the various  
396 soil layers, i.e. the capacity of the soil to resupply U in pore water.

### 397 3.3. R ratio for mine activity-related elements U and Pb

398 In this soil profile, since  $[U]_{DGT}$  values are as much as 15 times less than  $[U]_{DET}$  values, the  
399 corresponding R ratio ranges from 0.07 to 0.87 (Fig. 2). These results indicate that U  
400 resupply from soil layers to pore water evolves from a diffusion only case to a sustained case  
401 in response to the sink imposed by the DGT probe.

402 Over the first 26 cm, the R ratio remains globally constant at a low value ( $R_{0-26} = 0.19$ ,  
403 diffusion only case). The first peak in  $[U]_{DGT}$ , corresponding to layer L1, is perfectly  
404 mirrored with  $[U]_{DET}$ , resulting in a low R value. In fact, although the total U amount and  
405 water content are high in layer L1 (17.46 mg.kg<sup>-1</sup> and 85%, respectively), U mobility in this  
406 layer appears to be very low. This finding is consistent with the presence of OM soil particles  
407 and its well-known properties of complexing metals, thus leading to kinetically inert  
408 compounds in which U is tightly bound (Fuller et al. 2020, Stetten et al. 2018).

409 The second peak in  $[U]_{DGT}$  ( $R_{U,27-35} = 0.53$ , partially sustained case) corresponds to the L3  
410 and L3-4 layers, which appear to more readily transfer U to pore water than the other soil  
411 layers (DGT-labile species). As a reminder, layer L3 exhibits the highest stock of U (1,844  
412 mg.kg<sup>-1</sup>) and layer L3-4 is a transition zone displaying an evolution of texture from silt to  
413 sandy loam. For layer L2, with the same soil texture as L3, R remains constant at a low value  
414 ( $R_{U,12-18} = 0.19$ , diffusion only case). We can therefore conclude that the use of a DGT/DET  
415 combination in silt loam soil allows detecting the exchangeable U fraction.

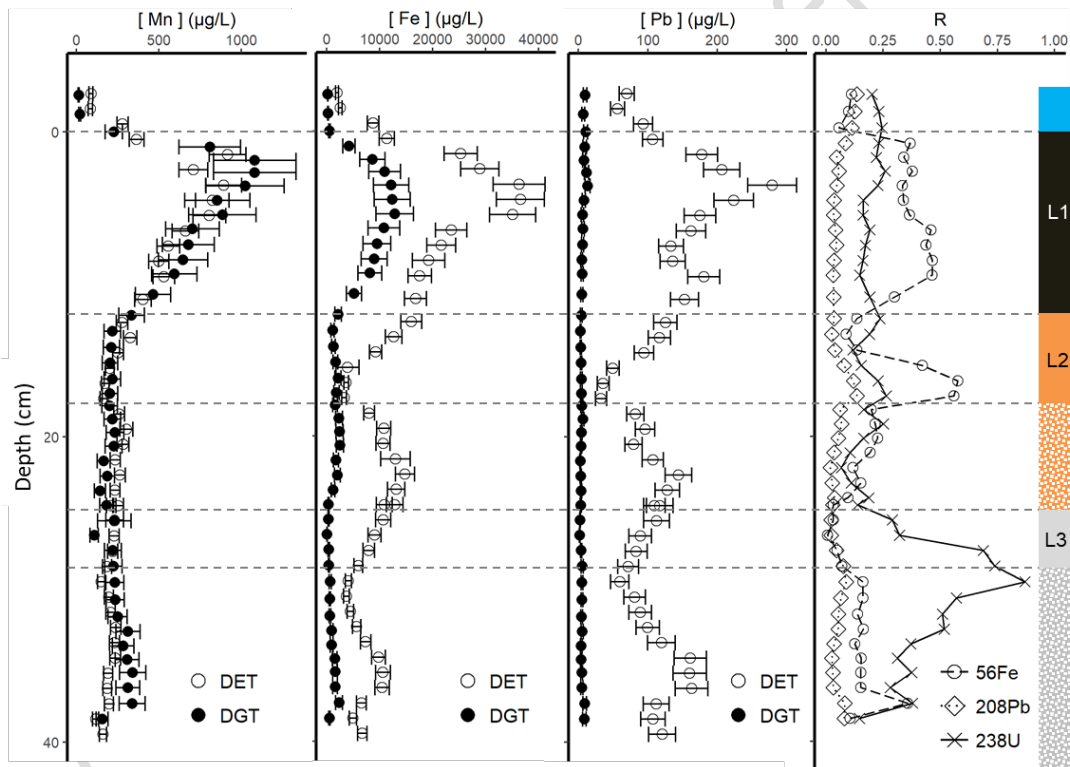
416 Given that U compounds appear to be exchangeable in layer L3, the case of Pb was also  
417 considered (Fig. 3). Lead is in fact a relevant indicator of mining activity known to be present  
418 here as a mixed U/Pb mineral (parsonsite) (Roux et al. 2020, Cuvier et al. 2016). Despite an  
419 initial increase of Pb concentration in pore water ( $[Pb]_{DET} = 279 \mu\text{g.L}^{-1}$ ) at 3.5 cm, like for  
420 U, no other variation was observed at the depths of U-impacted soil layers. The accumulation  
421 of Pb in DGT probes (after 24 h) is 7 to 50 times less than DET along the entire profile,  
422 leading to a poor resupply of Pb ( $R_{U,0-40} = 0.05$ ) from the soil layers close to a diffusion only



423 case. The difference between  $R_{Pb}$  and  $R_U$  profiles for mine-impacted layers (L3 and L3-4)  
 424 suggests that Pb, present into minerals, is immobilized as a non-DGT-labile form, whereas  
 425 U is present in a DGT-labile form capable of being resupplied from soil to pore water.

426 *3.4. Soil concentration profiles for red-ox sensitive elements (Mn, Fe) and implications for*  
 427 *U mobility*

428 In this final section, we examined the redox-sensitive contextual elements since uranium  
 429 speciation is strongly correlated with associated redox processes, e.g. the oxidation of  
 430 organic matter largely affected by microbial activities (Abdelouas 2006, Duff et al. 2002,  
 431 Coughlin and Hunter 2002). The DET and DGT depth profiles of Mn and Fe (Fig. 3) were  
 432 then acquired in order to characterize the redox conditions and potential acceptors of  
 433 electrons, as well as the metal resupply fluxes from soil to pore water.



434  
 435 Figure 3: DET and DGT depth profiles for Mn, Fe and Pb and comparison of R values for Fe, Pb  
 436 and U ; errors bars for Mn, Fe and Pb are 15%, 14% and 15% (for DET), 23%, 27% and 28% (for  
 437 DGT) and 27%, 31% and 32% (for R) respectively

438 Both  $[Mn]_{DET}$  and  $[Fe]_{DET}$  profiles show successive peaks located at 1.5-4 cm and 2.5-4.5  
 439 cm, respectively. The increase of  $[Mn]$  and  $[Fe]$  in pore water is generally interpreted as a  
 440

441 clue for the dissolution of Mn- and Fe-oxohydroxides by microbially-mediated reduction  
442 processes given their use as terminal electron acceptors in organic matter degradation  
443 processes (Thamdrup 2000, Fuller et al. 2020) after O<sub>2</sub> consumption below 1.5 cm (Fig. S6).

444 For Mn, the superimposition of both [Mn]<sub>DET</sub> and [Mn]<sub>DGT</sub> over the full depth profiles shows  
445 that Mn species are fully DGT-labile ( $R_{Mn,mean} = 1.1 \pm 0.3$ ), probably as Mn<sup>2+</sup> species  
446 dissolved in pore water. This is a typical sustained case whereby the solid phase easily  
447 resupplies pore water depleted by DGT. The few R variations observed in the R profile may  
448 be related to a constant, [Mn]<sub>soil</sub> (Table S8).

449 In the L1 top layer, Fe exhibits a different behavior. While its initial peak mirrors DET  
450 results, the R value is typical of a partially sustained case ( $R_{Fe,0-5} = 0.35$ ), meaning that the  
451 iron species are not fully exchangeable. Despite a very high content of total Fe ( $[Fe]_{soil,L1} =$   
452  $27.3 \text{ g.kg}^{-1}$ ), the presence of a high OM content acts as a trap by complexation, leading to  
453 potentially kinetically inert compounds. In layer L2, a fluctuation of R<sub>Fe</sub> between 10 and 18  
454 cm was observed, with a successive decrease from 0.47 to 0.09 and increase to 0.48. This  
455 sharp change occurred in a soil layer containing Fe-oxohydroxides (orange coloring) and  
456 reflects the alternation of a red-ox process. At this depth, it is likely that the seasonal  
457 variation in water table level (limit between oxic and anoxic zones) induces a change in the  
458 Fe speciation from insoluble Fe(III) to soluble and mobile Fe(II) species (Thamdrup 2000).

459 To summarize findings on the red-ox sensitive elements, the [Mn]<sub>DET</sub> and [Fe]<sub>DET</sub> profiles  
460 reveal a reductive mobilization of these metals just below the soil-water interface, in  
461 accordance with quick oxygen consumption. The initial increase in [U]<sub>DET</sub> and [U]<sub>DGT</sub>  
462 concentrations detected around 3.5 cm (Fig. 2) could thus be explained as the desorption of  
463 U trapped onto Fe- and Mn-oxohydroxides (Abdelouas 2006, Casiot et al. 2009) in a DGT-  
464 labile form. However, the resupply from soil to pore water is close to a diffusion only case,  
465 meaning that most of the U is trapped within the topsoil layer as kinetically inert complexes  
466 with OM.

467 As an additional experiment, the R value of the top soil layer (Fig S10) was investigated in  
468 November 2018 at the same location (with a slightly different soil profile). The first 3 cm of  
469 soil were completely dry compared to April 2018. [U]<sub>DET</sub> were then below the LQ preventing  
470 any correct R value calculation. From 3 cm to 10 cm, R values corresponding to low and  
471 high flow periods matched perfectly well ( $R = 0.17$  and  $0.18$  respectively). These results

472 show the L1 layer's capacity for complexing U whatever the season. In contrast in L2 layer,  
473 a seasonal process appears to take place as the low flow period R values (Nov.2018) increase  
474 (from 0.17 to 1) contrary to the high flow period R values (April 2018) suggesting that a red-  
475 ox process plays a major role in U lability. This result also demonstrates that U speciation in  
476 a wetland is driven by the water table level, which is in agreement with Stetten et al. (2018).

477 Lastly, two assumptions can be formulated in order to explain the mobility of an  
478 exchangeable U fraction in the L3 layer, identified as a residue of the former mining  
479 operations. First, some  $U_{VI}$  minerals (mined parsonsite and autunite) may remain  
480 undissolved in the L3 layer and constitute a stock of exchangeable U mobilized by the DGT  
481 sampling process as aqueous  $U_{VI}$  species (mineral dissolution). Second, a  $U_{IV}$ -exchangeable  
482 stock stemming from the reduction of these minerals may exist in the L3 layer (below the  
483 water table), and the DGT-labile fraction could be linked to the presence of mobile  $U_{IV}$ -  
484 bearing colloids (500 kDa - 0.22  $\mu$ m) constituted of  $Fe(OH)_2$  and OM (Stetten et al. 2018,  
485 Wang et al. 2013). Otherwise, the existence of seasonal red-ox fluctuations may also lead to  
486 a change in speciation from  $U_{IV}$ -immobilized (inert) species to  $U_{VI}$ -labile species (Stetten et  
487 al. 2018).

488

#### 489 4. Conclusion

490 An *in situ* methodology is proposed in order to assess metal resupply in a wetland soil,  
491 downstream of the former "Rophin" U mine. This methodology, which combines DET and  
492 DGT probes, presents numerous advantages, namely good spatial resolution, rapid  
493 equilibration time, robustness, ease of deployment and minimal soil disturbance;  
494 nonetheless, the *in situ* deployment in soil remains poorly documented. This work has  
495 highlighted the determination of metal resupply in a wetland from large soil profiles, in  
496 combination with detailed soil properties.

497 Our study confirms that this approach is applicable in soil layers with varying properties;  
498 only soil layers with low water content or coarse texture appear to be limiting factors. For  
499 soil profiles, DET provides new insight of the total dissolved Uranium species distribution  
500 along the pore water profile, whereas DGT highlights the presence of other "DGT labile"  
501 species such as dissociated and available organic complexes. The pairing of DET and DGT  
502 plus calculation of the R ratio, highlight two U behaviors in combining results from red-ox

503 sensitive elements (Mn and Fe). First, in the organic topsoil layer, an increase in  $[U]_{DET}$  and  
504  $[U]_{DGT}$  at 3-4 cm reflects the desorption of U trapped onto Fe- and Mn-oxohydroxides in a  
505 DGT-labile form. However, the resupply from soil to pore water is close to a diffusion only  
506 case ( $R < 0.2$ ), meaning that U is tightly bound by OM in the soil. Second, a peak in  $[U]_{DGT}$   
507 perfectly corresponding to the former mine deposit layer signifies the presence of U under  
508 DGT-labile species in comparison with other soil layers. Moreover, maximum R values of  
509 0.87 demonstrate the resupply of U from a labile fraction in this soil layer, as opposed to  
510 other elements like Pb.

511 In conclusion, all these information should be very helpful for interpreting data from any  
512 Uranium mining impacted wetlands similar to Rophin site.

513

## 514 5. Acknowledgments

515 The authors would like to thank Véronique Baty and Fiona Bouyer (SUBATECH) for their  
516 IC analysis and preliminary studies on DGT, respectively. Gratitude is also expressed to:  
517 Hafid Aglzim (SUBATECH) for GIS support; Dominique Demare (IFSTTAR) for the  
518 particle size distribution analysis of soil samples; Mathilde Zebracki (IRSN) for  
519 measurements of the  $O_2$  soil profile; Thierry Bataille (ENSCR) for XRD analysis; Sylvain  
520 Fresneau (SUBATECH) for production of the PVC holder; and Patrick Chardon (LPC),  
521 Hafid Aglzim, Andreas Fichtner and Fengqi Xu (SUBATECH) for their field technical  
522 support.

523 The authors are appreciative of the ZATU Pilot Workshop focusing on the Hercynian  
524 Orogeny (ZATU, <https://zatu.org/>), within the "Nantes-Atlantique" Sciences of the Universe  
525 Observatory (OSUNA, <https://osuna.univ-nantes.fr/>). The present study has been financially  
526 supported by the Loire Valley Regional Council (POLLUSOLS Project/OSUNA), as well  
527 as by the Carnot Mines/BRGM and Carnot Mines/UTOPIA programs. The authors are also  
528 thankful to the three anonymous reviewers for their constructive comments.

529

## 530 6. References

531 Abdelouas, A. 2006. "Uranium mill tailings: Geochemistry, mineralogy, and environmental  
532 impact." *Elements* 2 (6):335-341. doi: 10.2113/gselements.2.6.335.

- 533 Ahmed, H. M. M., 2014. "Lability and solubility of uranium and thorium in soil." PhD thesis,  
534 University of Nottingham (United Kingdom)
- 535 AREVA NC., 2009. Caractérisation géochimique des résidus de traitement de minerais  
536 d'uranium. Technical report. BUM/DI/QSSE CE 09/006 – PCN/MAN
- 537 Baize D., Girard M.-C., 2008. *Référentiel pédologique, Association française pour l'étude*  
538 *du sol (Afes)*. Edited by Quae.
- 539 Bond, D. L., Davis, J.A. Zachara. J.M., 2007. "Chapter 14 Uranium(VI) Release from  
540 Contaminated Vadose Zone Sediments: Estimation of Potential Contributions from  
541 Dissolution and Desorption." In *Developments in Earth and Environmental Sciences*,  
542 edited by Mark O. Barnett and Douglas B. Kent, 375-416. Elsevier.
- 543 Casiot, C., Egal M., Elbaz-Poulichet F., Bruneel, O., Bancon-Montigny C., Cordier M. A.,  
544 Gomez E., Aliaume C., 2009. "Hydrological and geochemical control of metals and  
545 arsenic in a Mediterranean river contaminated by acid mine drainage (the Amous  
546 River, France); preliminary assessment of impacts on fish (*Leuciscus cephalus*)." *Applied Geochemistry* 24 (5):787-799. doi: 10.1016/j.apgeochem.2009.01.006.
- 548 Chautard, C., Beaucaire C., Gerard M., Roy R., Savoye S., Descostes M., 2020.  
549 "Geochemical characterization of uranium mill tailings (Bois Noirs Limouzat,  
550 France) highlighting the U and 226Ra retention." *Journal of Environmental*  
551 *Radioactivity* 218 (March). doi: 10.1016/j.jenvrad.2020.106251.
- 552 Cuvier, A., Pourcelot L., Probst A., Prunier J., Le Roux G., 2016. "Trace elements and Pb  
553 isotopes in soils and sediments impacted by uranium mining." *Science of The Total*  
554 *Environment* 566-567:238-249. doi: 10.1016/J.SCITOTENV.2016.04.213.
- 555 Davison, W., 2016. *Diffusive Gradients in Thin-Films for Environmental Measurements*,  
556 *Cambridge Environmental Chemistry Series*. Cambridge: Cambridge University  
557 Press.
- 558 Di Bonito, M., Breward N., Crout N., Smith B., Young S., Zhang H., 2018. "Extraction and  
559 Characterization of Pore Water in Contaminated Soils." In, 195-235.
- 560 Docekal, B., Smetkova V., Docekalova H., 2003. "Characterization of Czech soils by  
561 diffusive gradients in thin films technique." *Chemical Papers* 57 (3):161-166.
- 562 Drozdak, J., Leermakers M., Gao Y., Phrommavanh V., Descostes M., 2015. "Evaluation  
563 and application of Diffusive Gradients in Thin Films (DGT) technique using Chelex  
564 (R)-100, Metsorb (TM) and Diphonix (R) binding phases in uranium mining  
565 environments." *Analytica Chimica Acta* 889:71-81. doi: 10.1016/j.aca.2015.07.057.
- 566 Drozdak, J., Leermakers M., Gao Y., Phrommavanh V., Descostes M., 2016. "Novel  
567 speciation method based on Diffusive Gradients in Thin Films for in situ  
568 measurement of uranium in the vicinity of the former uranium mining sites." *Environmental Pollution* 214:114-123. doi: 10.1016/j.envpol.2016.04.004.
- 570 Duff, M. C., Coughlin J.U., Hunter D.B., 2002. "Uranium co-precipitation with iron oxide  
571 minerals." *Geochimica Et Cosmochimica Acta* 66 (20):3533-3547. doi:  
572 10.1016/s0016-7037(02)00953-5.
- 573 Duquene, L., Vandenhove H., Tack F., Van Hees M., Wannijn J., 2010. "Diffusive gradient  
574 in thin Films (DGT) compared with soil solution and labile uranium fraction for  
575 predicting uranium bioavailability to ryegrass." *Journal of Environmental*  
576 *Radioactivity* 101 (2):140-147. doi: 10.1016/j.jenvrad.2009.09.007.

- 577 Fuller, A. J., Leary P., Gray N.D., Davies H.S., Mosselmans J.F.W., Cox F., Robinson C.H.,  
578 Pittman J.K., McCann C.M., Muir M., Graham M.C., Utsunomiya S., Bower W.R.,  
579 Morris K., Shaw S., Bots P., Livens F.R., Law G.T.W., 2020. "Organic complexation  
580 of U(VI) in reducing soils at a natural analogue site: Implications for uranium  
581 transport." *Chemosphere* 254:126859. doi: 10.1016/j.chemosphere.2020.126859.
- 582 Gao, Y., Baeyens W., De Galan S., Poffijn A., Leermakers M., 2010. "Mobility of radium  
583 and trace metals in sediments of the Winterbeek: Application of sequential extraction  
584 and DGT techniques." *Environmental Pollution* 158 (7):2439-2445. doi:  
585 10.1016/j.envpol.2010.03.022
- 586 Gao, Y., Leermakers M., Gabelle C., Divis P., Billon G., Ouddane B., Fischer J.C., Wartel  
587 M., Baeyens W., 2006. "High-resolution profiles of trace metals in the pore waters  
588 of riverine sediment assessed by DET and DGT." *Science of the Total Environment*  
589 362 (1-3):266-277. doi: 10.1016/j.scitotenv.2005.11.023.
- 590 Gregusova, M., Docekal B., 2011. "New resin gel for uranium determination by diffusive  
591 gradient in thin films technique." *Analytica Chimica Acta* 684 (1-2):142-146. doi:  
592 10.1016/j.aca.2010.11.002.
- 593 Guan, D.-X., 2019. "Diffusive Gradients in Thin-Films (DGT): An Effective and Simple  
594 Tool for Assessing Contaminant Bioavailability in Waters, Soils and Sediments." In  
595 *Encyclopedia of Environmental Health (Second Edition)*, edited by Jerome Nriagu,  
596 111-124. Oxford: Elsevier.
- 597 Heiri, O., Lotter A.F., Lemcke G., 2001. "Loss on ignition as a method for estimating organic  
598 and carbonate content in sediments: reproducibility and comparability of results."  
599 *Journal of Paleolimnology* 25 (1):101-110. doi: 10.1023/a:1008119611481.
- 600 Hooda, P. S., Zhang H., Davison W., A. C. Edwards A.C., 1999. "Measuring bioavailable  
601 trace metals by diffusive gradients in thin films (DGT): soil moisture effects on its  
602 performance in soils." *European Journal of Soil Science* 50 (2):285-294. doi:  
603 10.1046/j.1365-2389.1999.00226.x.
- 604 Kohler, M., Curtis G.P., Meece D.E., Davis J.A., 2004. "Methods for Estimating Adsorbed  
605 Uranium(VI) and Distribution Coefficients of Contaminated Sediments."  
606 *Environmental Science & Technology* 38 (1):240-247. doi: 10.1021/es0341236.
- 607 Krom, M., 1994. "High Resolution Sampling of Pore Waters Using a Gel Probe from  
608 Esthwaite Water, Lake District." *Mineralogical Magazine - MINER MAG* 58A:497-  
609 498. doi: 10.1180/minmag.1994.58A.1.259.
- 610 Leermakers, M., Gao Y., Gabelle C., Lojen S., Ouddane B., Wartel M., Baeyens W., 2005.  
611 "Determination of high resolution pore water profiles of trace metals in sediments of  
612 the Rupel River (Belgium) using DET (diffusive equilibrium in thin films) and DGT  
613 (diffusive gradients in thin films) techniques." *Water Air and Soil Pollution* 166 (1-  
614 4):265-286. doi: 10.1007/s11270-005-6671-7.
- 615 Leermakers, M., Phrommavanh V., Drozdak J., Gao Y., Nos J., Descostes M., 2016. "DGT  
616 as a useful monitoring tool for radionuclides and trace metals in environments  
617 impacted by uranium mining: Case study of the Sagnes wetland in France."  
618 *Chemosphere* 155:142-151. doi: 10.1016/j.chemosphere.2016.03.138.
- 619 Lottermoser, B. G, Ashley P. M., 2005. "Tailings dam seepage at the rehabilitated Mary  
620 Kathleen uranium mine, Australia." *Journal of Geochemical Exploration* 85 (3):119-  
621 137. doi: 10.1016/j.gexplo.2005.01.001.

- 622 Martin, A., Hassan-Loni Y., Fichtner A., Péron O., David K., Chardon P., Larrue S.,  
623 Gourgiotis A., Sachs S., Arnold T., Grambow B., Stumpf T., Montavon G., 2020.  
624 "An integrated approach combining soil profile, records and tree ring analysis to  
625 identify the origin of environmental contamination in a former uranium mine  
626 (Rophin, France)." *Science of The Total Environment* 747:141295. doi:  
627 10.1016/j.scitotenv.2020.141295.
- 628 Monbet, P., McKelvie I. D., Worsfold P. J., 2008. "Combined gel probes for the in situ  
629 determination of dissolved reactive phosphorus in porewaters and characterization  
630 of sediment reactivity." *Environmental Science & Technology* 42 (14):5112-5117.  
631 doi: 10.1021/es8001663.
- 632 Nowack, B., Koehler S., Schulin R., 2004. "Use of Diffusive Gradients in Thin Films (DGT)  
633 in Undisturbed Field Soils." *Environmental Science & Technology* 38 (4):1133-1138.  
634 doi: 10.1021/es034867j.
- 635 Pradit, S., Gao Y., Faiboon A., De Galan S., Baeyens W., Leermakers M., 2013.  
636 "Application of DET (diffusive equilibrium in thin films) and DGT (diffusive  
637 gradients in thin films) techniques in the study of the mobility of sediment-bound  
638 metals in the outer section of Songkhla Lake, Southern Thailand." *Environmental*  
639 *Monitoring and Assessment* 185 (5):4207-4220. doi: 10.1007/s10661-012-2862-z.
- 640 Peijnenberg, J.G.M., Teasdale P.R., Reible D., Mondon J., Bennett W.W., Campbell P. G.C.,  
641 2014. "Passive Sampling Methods for Contaminated Sediments: State of the Science  
642 for Metals." *Integrated Environmental Assessment and Management* 10(2):179-  
643 196 published by Wiley Periodicals
- 644 Roux, C., Grangeon S., Lerouge C., Chardon P., Beuzeval R., Montavon G., Grangeon T.,  
645 Claret F., 2020. "Geochemical characterization of radionuclides and associated trace  
646 elements (As, Ba, Li, Pb, Sr, Zn) downstream a former uranium mine (Rophin,  
647 France)." Submitted to *Applied Geochemistry*.
- 648 Sajih, M., Bryan N. D., Livens F. R., Vaughan D. J., Descostes M., Phrommavanh V., Nos  
649 J., Morris K., 2014. "Adsorption of radium and barium on goethite and ferrihydrite:  
650 A kinetic and surface complexation modelling study." *Geochimica et Cosmochimica*  
651 *Acta* 146:150-163. doi: 10.1016/j.gca.2014.10.008.
- 652 Schöner, A., Noubactep C., Sauter M., 2009. "Geochemistry of natural wetlands in former  
653 uranium milling sites (eastern Germany) and implications for uranium retention."  
654 *Geochemistry* 69:91-107. doi: 10.1016/j.chemer.2007.12.003.
- 655 Stetten, L., Blanchart P., Mangeret A., Lefebvre P., Le Pape P., Brest J., Merrot P., Julien  
656 A., Proux O., Webb S.M., Bargar J.R., Cazala C., Morin G., 2018. "Redox  
657 Fluctuations and Organic Complexation Govern Uranium Redistribution from  
658 U(IV)-Phosphate Minerals in a Mining-Polluted Wetland Soil, Brittany, France."  
659 *Environmental Science & Technology* 52 (22):13099-13109. doi:  
660 10.1021/acs.est.8b03031.
- 661 Thamdrup, B., 2000. "Bacterial Manganese and Iron Reduction in Aquatic Sediments." In  
662 *Advances in Microbial Ecology*, edited by Bernhard Schink, 41-84. Boston, MA:  
663 Springer US.
- 664 Turner, G. S. C., Mills G. A., Teasdale P. R., Burnett J. L., Amos S., Fones G. R., 2012.  
665 "Evaluation of DGT techniques for measuring inorganic uranium species in natural

- 666 waters: Interferences, deployment time and speciation." *Analytica Chimica Acta*  
667 739:37-46. doi: 10.1016/j.aca.2012.06.011.
- 668 Ullah, S., Zhang H., Heathwaite A. L., Binley A., Lansdown K., Heppell K., Trimmer M.,  
669 2012. "In situ measurement of redox sensitive solutes at high spatial resolution in a  
670 riverbed using Diffusive Equilibrium in Thin Films (DET)." *Ecological Engineering*  
671 49:18-26. doi: 10.1016/j.ecoleng.2012.08.003.
- 672 Wang, Y., Bagnoud A., Suvorova E., McGivney E., Chesaux L., Phrommavanh V.,  
673 Descostes M., Bernier-Latmani R., 2014. "Geochemical Control on Uranium(IV)  
674 Mobility in a Mining-Impacted Wetland." *Environmental Science & Technology* 48  
675 (17):10062-10070. doi: 10.1021/es501556d.
- 676 Wang, Y., Frutschi M., Suvorova E., Phrommavanh V., Descostes M., Osman A.A.A.,  
677 Geipel G., Bernier-Latmani R., 2013. "Mobile uranium(IV)-bearing colloids in a  
678 mining-impacted wetland." *Nature Communications* 4 (May):1-9. doi:  
679 10.1038/ncomms3942.
- 680 Zachara, J., Liu C., Brown C., Kelly S., Christensen J., McKinley J., Davis J.A., Serne J.,  
681 Dresel E., Um W. "A Site-Wide Perspective on Uranium Geochemistry at the  
682 Hanford Site" 2007, Pacific Northwest National Laboratory report PNNL-17031
- 683 Zhang, H., Davison W., 1995. "Performance-Characteristics of diffusion gradients in thin-  
684 films for the in-situ measurement of trace-metals in aqueous solution." *Analytical*  
685 *Chemistry* 67 (19):3391-3400. doi: 10.1021/ac00115a005.